Research Square

Preprints are preliminary reports that have not undergone peer review.
They should not be considered conclusive, used to inform clinical practice,
or referenced by the media as validated information.

Core microbiota recruited by Salvia miltiorrhiza enhance resistance against Fusarium root rot disease

Chuan You
Nanjing Agricultural University
Yang Gao
gaoyang@njau.edu.cn

Nanjing Agricultural University
Peng Ren
Nanjing Agricultural University
Weiqi Zhang
Nanjing Agricultural University
Kai Gong
Nanjing Agricultural University
Qin Zhang
Nanjing Agricultural University
Xingchang Wang
Guizhou University
Wuxian Zhou
Nanjing Agricultural University
Rolf Kümmerli
University of Zurich
Yangchun Xu
Nanjing Agricultural University
Qirong Shen
Nanjing Agricultural University
Zhong Wei
Nanjing Agricultural University
Xiaofang Wang
Nanjing Agricultural University

Article

Keywords: Fusarium root rot, Lysobacter enzymogenes, Rhizosphere microbiome, Iron competition, Siderophore

Posted Date: October 26th, 2026

DOI: https://doi.org/10.21203/rs.3.rs-10633457/v1

License: This work is licensed under a Creative Commons Attribution 4.0 International License. Read Full License

Additional Declarations: No competing interests reported.

Abstract

Fusarium root rot, caused by the soilborne pathogen *Fusarium oxysporum*, leads to substantial yield losses across multiple agriculturally crucial crops. While rhizosphere microbiota have been extensively studied in model species, a deeper understanding of the rhizosphere microbiome assembly associated with herb health is still needed. Given its economic importance in traditional medicine, we used *Salvia miltiorrhiza* and *Fusarium* root rot as a model to elucidate the rhizosphere microbiome assembly associated with plant health. Here, we employed 16S rRNA amplicon sequencing to profile the soil microbiome across three geographically distinct cultivation regions. Comparative analysis revealed marked divergence in bacterial community structures between healthy and diseased plants, identifying *Lysobacter* spp. as keystone bacterial taxa within the core microbiome enriched in healthy rhizospheres. Functional validation demonstrated potent antifungal activity of isolated *Lysobacter* strains against *F. oxysporum*, with *Lysobacter enzymogenes* strain Ly-1 exhibiting consistent biocontrol efficacy in both greenhouse and field experiments. Genomic and transcriptomic analyses further revealed that Ly-1 encodes specialized iron acquisition systems, including siderophore synthesis and transport machinery, with its antifungal activity being significantly amplified under iron-limited conditions, consistent with a model where iron competition cooperates with other biocontrol traits. Collectively, this study establishes a novel biocontrol paradigm and highlights the translational potential of core rhizobacterial enrichment for sustainable management of soilborne diseases in medicinal plants.

Introduction

Soil-borne root rot diseases pose a critical threat to global agricultural productivity, causing substantial yield losses and quality deterioration in economically crucial crops [1]. While most researches focused on staple food crops, *Salvia miltiorrhiza* Burge (Danshen)- a perennial medicinal herb valued for producing bioactive compounds (tanshinone I, tanshinone II, miltirone and salvianolic acid)- faces unique challenges as a root-based medicinal crop [2–3]. The underground rhizomes of *S. miltiorrhiza*, which accumulate pharmaceutically valuable metabolites, are reported to suffer yield losses up to 40% by *Fusarium oxysporum*-mediated root rot under intensive monoculture systems [4–5]. This devastating disease manifests as root necrosis, vascular browning and systemic wilting, ultimately compromising both biomass production and secondary metabolite biosynthesis [6].

These rhizosphere-associated microorganisms enhance plant fitness by facilitating nutrient acquisition, modulating host immune responses, and competitively excluding soil-borne pathogens [7]. Notably, plants actively shape their rhizosphere microbiomes, resulting in species-specific microbial assemblages even when grown in identical soils-a phenomenon termed the “rhizosphere effect” [8]. While previous studies have focused on characterizing disease-suppressive microbiomes in monoculture cropping systems from single geographic regions, whether core microbiota function across soil types remains unclear. Soil physicochemical properties and microbial communities often exhibit substantial spatial heterogeneity across agricultural fields, even within the same farming system. Emerging evidence suggests that conserved core microbiota in the rhizosphere may contribute to

pathogen suppression, irrespective of soil type [9]. Existing biocontrol agents against soil-borne pathogens often suffer from inconsistent field efficacy due to host-specificity limitations and environmental variability [10]. This underscores the urgency of developing host-adapted microbial solutions through mining the indigenous rhizosphere microbiome of *S. miltiorrhiza*.

Emerging evidence suggests that rhizosphere core microbiota can form disease-suppressive soils through multiple mechanisms, including nutrient competition and antimicrobial compound production [11]. Nutrient competition, particularly for carbon sources and iron, is crucial in microbial interactions. Microorganisms compete for these resources through mechanisms like siderophore production, which helps acquire iron [12]. In addition, antagonistic competition involves the secretion of bioactive compounds such as antibiotics or lytic enzymes that inhibit pathogen growth [13]. These strategies enable microorganisms to secure essential nutrients and limit pathogen survival, enhancing their own growth and colonization success in various environments. Moreover, these disease-suppressive mechanisms often function synergistically, with microbes integrating nutrient competition and antimicrobial secretion to build multi-layered defense networks. A deeper understanding of these interactive processes will facilitate the development of microbiome-based, eco-friendly strategies for disease control.

We hypothesized that *S. miltiorrhiza* recruits specialized rhizosphere microbiota to counteract *F. oxysporum* invasion. To test this, we conducted a multi-omics investigation across three major production regions (purple, cinnamon, and brown soils) under long-term monoculture of *S. miltiorrhiza* in China. Comparative 16S rRNA profiling of healthy versus diseased rhizospheres identified *Lysobacter* as a conserved keystone taxon in suppressive soils. Functional characterization of the antagonistic strain *L. enzymogenes* Ly-1 combined genomic and transcriptomic analyses to decipher its iron-scavenging machinery. Through integrated greenhouse and field experiments, we demonstrate that Ly-1's siderophore-mediated competition, establishing a biocontrol paradigm for medicinal plant protection.

Results

Soil physicochemical properties and pathogen dynamics in S. miltiorrhiza rhizosphere

We established a paired-field sampling strategy across three geographically distinct production regions (Site FY, SJZ and CD), each containing adjacent fields with contrasting disease incidence: severely root rot diseased (D) versus healthy (H) *S. miltiorrhiza* stands (Fig. 1a, b). The workflow for this study was shown in Fig. S1a. Compared to healthy soils, diseased soils exhibited a significantly higher abundance of *F. oxysporum* (Fig. 1c). Compared to diseased soils, healthy soils exhibited significantly higher pH ($P < 0.01$, Wilcoxon test) and cation exchange capacity (CEC) ($P < 0.001$, Wilcoxon test) on average (Fig. S2, Table S1). In contrast, diseased soils exhibited a significantly higher abundance of nitrite nitrogen (NO_3-N) ($P < 0.001$, Wilcoxon test), ammonia nitrogen (NH_4-N) ($P < 0.001$, Wilcoxon test), available potassium (AK) ($P < 0.05$, Wilcoxon test) and available iron (Fe) ($P < 0.001$, Wilcoxon test) compared to healthy soils

(Fig. S2, Table S1). Together these results suggest that the soil physicochemical properties varied between the diseased and healthy plant rhizosphere.

Disease-driven restructuring of rhizobacterial communities

To further investigate the differences in bacterial communities between healthy and diseased rhizospheres, we utilized 16S rRNA amplicon sequencing. In total, 53,335 bacterial ASVs (97% similarity threshold) from 30 rhizosphere samples. Principal co-ordinates analysis (PCoA) showed that both sample locations and plant-healthy status affect the composition of bacterial community (Adonis, site: R^2 = 0.23, P = 0.001; D/H status: R^2 = 0.10, P = 0.001, site × D/H: R^2 = 0.11, P = 0.002, Fig. 1d). Nevertheless, both the observed species number and shannon index did not differ between groups (Wilcoxon test, P > 0.05, Fig. S3 a and b). This dissociation suggests that root rot pathogenesis in *S. miltiorrhiza* is mediated primarily by compositional reorganization of rhizobacterial assemblages, not by gross diversity alterations. Proteobacteria, Acidobacteriota and Actinobacteriota were the dominant bacterial taxa at the phylum level (Fig. 1e). Root rot significantly increased the abundance of Proteobacteria but reduced the abundance of Acidobacteriota.

Key bacterial taxa in the healthy rhizosphere of S. miltiorrhiza are largely independent of geography

To identify core rhizosphere bacteria in *S. miltiorrhiza*, we systematically ranked bacterial genera based on their average relative abundance across healthy (H) and diseased (D) samples. High-abundance core taxa were defined as those meeting dual criteria: 1) average relative abundance ≥ 0.5%, and 2) consistent detection in all three geographical regions. This stringent selection identified 29 bacterial genera shared among 30 H and D samples (Fig. 2a and S4). Subsequent comparative analysis revealed 12 genera with significant enrichment in healthy rhizosphere soils from different sites (Log_2 fold change > 1, P < 0.05, Fig. 2b). Notably, *Lysobacter* enrichment was consistent across sites, demonstrating both significant abundance differences across all three locations (Log_2FC > 1, P < 0.05, Fig. 2c) and consistently higher relative abundance in healthy soils (Fig. 2d). While geographical variation influenced overall bacterial community structure, its effect on *Lysobacter* distribution was comparatively minor. This differential response suggests that *Lysobacter* abundance is primarily driven by plant health status rather than geographical factors.

Biocontrol potential of identified Lysobacter isolates against Fusarium root rot in S. miltiorrhiza

The workflow for this study was shown in Fig.S1b. To elucidate the biocontrol potential of *Lysobacter* against *Fusarium*-related root rot, four antagonistic strains were isolated from healthy *S. miltiorrhiza* rhizospheres. Notably, strain Ly-1 exhibited superior antifungal activity, forming inhibition zones > 10 mm against *F. oxysporum* 220 (Fig. S5), prompting its selection for in-depth characterization. Phylogenetic analysis of the 16S rRNA gene revealed 97% sequence similarity with *Lysobacter enzymogenes* 521 (Fig. 3a). A greenhouse experiment showed that the application of Ly-1 significantly reduced root rot pathogenesis, reducing disease indices by 38.9% compared to controls (Fig. 3b and d). This biocontrol

efficacy correlated with *F. oxysporum* abundance reduction in rhizosphere soils (Fig. 3e). Despite minimal field disease incidence, both pot and field experiments consistently demonstrated Ly-1's growth-promoting effects: treated plants exhibited 21.3% and 17.8% increases in aboveground and underground biomass, respectively (Fig. 3c, f, g and Fig. S6). Together these results indicated that Ly-1's dual functionality-not only suppressing *F. oxysporum* proliferation but also enhancing *S. miltiorrhiza* productivity. The dissociation between disease suppression and biomass enhancement under field conditions suggests additional plant growth-promoting mechanisms beyond direct pathogen inhibition.

L. enzymogenes Ly-1 suppresses F. oxysporum growth via iron-chelating siderophore secretion

The workflow for this study was shown in Fig.S1c. We first investigated the correlation between different physicochemical factors of rhizosphere soil and the number of *F. oxysporum*, and the results showed that iron ion content was a key factor affecting the number of *F. oxysporum* (Fig. 4a; $R^2 = 0.707$, $P < 0.001$). We hypothesized that *Lysobacter* suppressed *F. oxysporum* by influencing rhizosphere Fe^{3+} content. To test this hypothesis, a causal model was constructed, and three different methods-random common cause refuter, placebo treatment refuter, and data subset refuter-were employed to verify and refute the hypothesis. The results showed, regardless of whether the averaging approach or clustered multiple threshold approach was used, the P-values from all three refutation methods were much greater than 0.05. This led to the conclusion that the null hypothesis could not be rejected, suggesting that rhizosphere Fe^{3+} content may serve as one of the key mediators through which *Lysobacter* suppresses *F. oxysporum*, in addition to other antagonistic mechanisms such as antibiotic production and cell-wall-degrading enzymes (Fig. 4b). To elucidate the molecular basis of biocontrol ability in *L. enzymogenes* Ly-1, we integrated second- and third-generation sequencing to assemble its complete genome. Nanopore sequencing generated 6,666,776 high-quality reads (average length: 5,779 bp; N50: 6,328 bp), while Illumina produced 1,020 Mbp of clean data (Q30: 95.6%). The circular chromosome spans 6,270,474 bp (GC content: 68.98%) and encodes 15,231 genes, including 77 linked to biocontrol and plant growth promotion (e.g., siderophores, iron transport, chitinase; Fig. 4c). KEGG annotation further identified biosynthetic clusters for antibiotics, terpenoids, and nonribosomal peptides (Table S2). To validate the functional importance of iron in *F. oxysporum* growth, we performed iron supplementation assays in iron-limited MKB medium. Fungal biomass exhibited a dose-dependent response to Fe^{3+} content (Fig. 4d), confirming iron's critical role in pathogen proliferation. Functional validation via CAS assays confirmed iron-responsive siderophore secretion, with significantly higher production under iron-limited conditions. Intriguingly, supernatants from iron-limited cultures (containing maximal siderophores) significantly inhibited *F. oxysporum* growth (Fig. 4e), suggesting auxiliary antifungal mechanisms. We analyzed transcriptomic responses of Ly-1 grown under iron-limited condition versus iron-rich condition. Comparative RNA-seq revealed substantial transcriptional reprogramming, with 328 genes upregulated and 572 downregulated ($|\log_2 FC| > 1$, FDR < 0.05; Fig. 4f). KEGG pathway analysis demonstrated iron-limited condition-induced functions, including significant enrichment of ribosome, two-component system, D-Amino acid metabolism, biosynthesis of various antibiotics, oxidative phosphorylation, amino sugar and nucleotide sugar metabolism, sulfur metabolism, biosynthesis of siderophore group

nonribosomal peptides, pentose phosphate pathway, and ABC transporters pathways (Fig. 4g). Then, Ly-1 was inoculated onto CAS agar plates and incubated statically for 4 d, resulting in the formation of yellow halos around the colonies (Fig. S7a). When cultured in iron-limited MKB medium for 48 h, the siderophore-containing supernatant was mixed with CAS detection solution, and the solution changed from blue to light red (Fig. S7b), confirming that Ly-1 produces siderophores under iron-limited conditions. In silico analysis using the SIDERITE database predicted Lysocin E, a 37-membered depsipeptide with known bactericidal activity, in Ly-1 supernatants (Fig. S8). These results suggested that the biocontrol activity of *L. enzymogenes* Ly-1 against *F. oxysporum* in the rhizosphere involves a combination of iron deficiency-induced siderophore secretion and the production of antibiotics and lytic enzymes, which collectively restrict pathogen proliferation.

Discussion

Advances in high-throughput sequencing have revolutionized our capacity to decode crop-associated microbiomes, enabling the identification of core microbial taxa with pathogen-suppressive potential [13, 14]. In this study, a comparative analysis revealed a significant enrichment of *Lysobacter* spp. in the rhizosphere microbiome of healthy (H) soils compared to diseased (D) soils. Through integrated phenotypic and genomic investigations, we further demonstrated that *Lysobacter* strains directly inhibit *Fusarium oxysporum* invasion via multiple mechanisms, including iron competition and antifungal metabolite production. Our study extends this paradigm by demonstrating that *Lysobacter* Ly-1, isolated from *S. miltiorrhiza* rhizosphere, directly inhibits *F. oxysporum* colonization in planta. Unlike previous reports focusing on indirect suppression via systemic resistance, we provide mechanistic evidence that Ly-1 restricts *Fusarium* proliferation at the rhizosphere interface through a multifaceted strategy involving siderophore-mediated iron competition, antibiotic secretion, and lytic enzyme production, significantly reducing root rot severity. These findings highlight the potential of *Lysobacter* as a keystone taxon in engineering pathogen-suppressive rhizosphere microbiomes.

Maintaining microbial community equilibrium is critical for sustaining beneficial host-microbe interactions. Dysbiosis-characterized by both the enrichment of detrimental taxa and depletion of protective microbes-serves as a key driver of plant disease development [15]. Notably, certain taxa like *Lysobacter* exhibit broad-spectrum pathogen suppression, positioning them as critical regulators of rhizosphere health. *Lysobacter* spp., a small branch within the phylum Proteobacteria, possesses strong ecological adaptability and is widely distributed in terrestrial and aquatic ecosystems, as well as host-associated habitats such as the plant rhizosphere [16]. They have strong colonization abilities in the rhizosphere and can secrete various antibiotics and extracellular hydrolytic enzymes, exhibiting lytic activity against a wide range of pathogenic fungi and bacteria [17–18]. Members of this genus, including *L. antibioticus*, *L. capsici*, and *L. gummosus*, enhance plant resilience through multifaceted mechanisms. *Lysobacter* spp. can produce antimicrobial compounds (e.g., lysobactin, lactivicin, and heat-stable antifungal factor [HSAF]) [19–22], combined with predatory activity against bacteria, fungi, nematodes and oomycetes[23–24]. Moreover, they can induce systemic resistance and growth promotion via phytohormone signaling [25]. These functional traits likely explain the selective enrichment of *Lysobacter*

in pathogen-challenged rhizospheres. For example, *L. capsici* strain NF87, enriched in disease-resistant green pepper rhizospheres, suppresses *Rhizoctonia solani* through secondary metabolite secretion [26].

The rhizosphere, a dynamic interface between plant roots and soil, sustains remarkably dense microbial populations that modulate iron bioavailability and pathogen suppression in plant health [27]. Iron competition represents a pivotal microbial warfare strategy in the iron-limited rhizosphere niche. As an essential cofactor in cellular processes such as photosynthesis, respiration, and electron transfer, iron bioavailability governs both pathogen virulence and microbial community dynamics [28]. Bacteria employ sophisticated iron acquisition systems, particularly siderophore-mediated chelation, to outcompete pathogens for this scarce resource [29]. Siderophores are low-molecular-weight iron chelators (with a molecular weight of less than 1 kDa) that have a high affinity for Fe^{3+} [30]. Bacterial siderophores can be synthesized via non-ribosomal peptide synthetase (NRPS), polyketide synthase (PKS) modules, or NRPS/PKS-independent pathways and exhibit superior Fe^{3+} affinity, enabling effective iron sequestration from fungal competitors [31]. For example, pseudobactin from *Pseudomonas syringae* BAF.1 exhibited 95.24% growth inhibition against *Fusarium oxysporum* under iron deprivation conditions [32], highlighting the therapeutic potential of iron competition strategies.

Pathogenic fungi require iron to synthesize many crucial biological molecules, such as cytochromes and certain enzymes [33]. Studies have shown that in soil environments, the availability of iron (i.e., the concentration of dissolved iron) is closely related to the growth and pathogenicity of these fungi [34–35]. When the concentration of iron ions in the soil is high, certain plant pathogens (such as *Botrytis cinerea*, *Fusarium oxysporum*, etc.) are able to grow and reproduce better, which enhances their pathogenicity toward host plants. Supporting this mechanism, previous studies demonstrated that iron acquisition blockade effectively inhibits *F. oxysporum* infection and mycelial proliferation in murine models [36]. Our experimental data corroborate the critical importance of iron availability, showing significant enhancement of *F. oxysporum* growth under iron-replete conditions. Several beneficial *Lysobacter* species have demonstrated the ability to suppress pathogens through indirect mechanisms such as nutrient competition. Notably, certain *Lysobacter* strains exhibit facultative predatory behaviors analogous to myxobacteria, employing antagonistic strategies under nutrient-limited conditions [37–39]. Genomic evidence further indicates that Ly-1 may directly antagonize *F. oxysporum* through chitinase and β-glucosidase production while simultaneously synthesizing siderophores to sequester scarce iron ions. Transcriptomic analysis revealed that iron-limited conditions induced in Ly-1 a broad stress-adaptation response, with KEGG pathways significantly enriched for ribosome, two-component system, biosynthesis of siderophore group nonribosomal peptides, various antibiotics, and amino sugar metabolism. This molecular profile supports the genomic inference that Ly-1 antagonizes *F. oxysporum* not only directly via chitinase and β-glucosidase but also by competitively synthesizing siderophores under iron scarcity. Overall, these results indicate that *Lysobacter* employs a multifaceted strategy to inhibit *F. oxysporum* invasion in the *S. miltiorrhiza* rhizosphere. This strategy integrates siderophore-mediated iron competition, antibiotic production, and cell-wall-degrading enzymes such as chitinase and β-glucosidase, which act synergistically to restrict pathogen growth and colonization.

Many beneficial bacteria can influence the iron acquisition ability of pathogens through competition, bacteriocin production, or secretion of specific molecules, thereby inhibiting the growth and pathogenicity of pathogens. For example, lactic acid bacteria can directly inhibit pathogens growth by synthesizing bacteriocins, while also competitively acquiring iron from the host or environment through specific low molecular weight iron-binding proteins, limiting the iron sources available to pathogens and thus inhibiting their growth [40]. *Escherichia coli* synthesizes siderophores (such as tyrosine-derived compounds) to competitively bind iron and inhibit the synthesis of iron transporters in other pathogens, reducing their pathogenicity [41]. This finding contrasts with conventional rhizosphere competition dynamics, where beneficial microbes typically suppress pathogens through siderophore-mediated iron scavenging [12]. Intriguingly, our iron limitation experiments revealed unexpected growth patterns of *F. oxysporum* in Ly-1 supplemented media, suggesting potential interspecific interactions beyond simple resource competition. Recent investigations into *Lysobacter enzymogenes* have identified lysochelin [N1, N8-bis(2,3-dihydroxybenzoyl) spermidine] as its primary siderophore, with spermidine and HSAF biosynthesis being iron-regulated and critical for bacterial survival [42–44]. Building on these discoveries, we characterized a potential siderophore (Lysocin E) and its associated biosynthetic gene cluster in *L. enzymogenes*. This molecule, as an antimicrobial peptide antibiotic, has strong anti-microbial activity by destroying the cell wall [45]. Due to the importance of siderophores and the challenges associated with their synthesis and separation, future studies should focus on functional validation of these genetic elements and quantitative assessment of Lysocin E production under varying iron conditions.

Collectively, by examining six separate field locations, we were able to identify consistent microbiome signatures related to disease suppressiveness (Fig. 5). this study presents a case highlighting rhzosphere protection of *S. miltiorrhiza* plant from under-ground rot disease by beneficial rhizosphere bacteria. Utilizing the advantageous properties of rhizosphere *Lysobacter* may present potential strategies to improve the growth and resilience of herb plants in agricultural settings.

Materials and Methods

Experimental design and sampling

In October 2023, a field disease survey of large-scale medicinal garden (> 5 ha) was conducted to detect root rot disease among the *S. miltiorrhiza* plantations in Fuyang, Anhui province (altitude: 17.7 m, 115°24 E, 33°06 N), Shijiazhuang, Hebei province (altitude: 128.6 m, 114°48 E, 38°03 N), and Chengdu, Sichuan province (altitude: 503.2 m, 104°06 E, 30°67 N), the main *S. miltiorrhiza* production area in China, where low-altitude climatic conditions and slightly arid and acidic soil conditions dictate the timing of autumn *S. miltiorrhiza* harvests. To minimize the effects of cultivar, cropping year, growing period, and microclimate in the natural environment, plants with both healthy and root rot symptoms of root rot disease that were collected during the same year with the same cultivar (*Salvia miltiorrhiza* Bunge) in this study. Five representative subplots were sampled from each field. Within each subplot, two paired plants were sampled and pooled as a composite sample.

Measurement of rhizosphere soil chemical properties

The physical and chemical properties of the soil were measured from healthy and diseased soil samples harvested in the field, as mentioned above. For pH analysis, soils were extracted in deionized water for one hour to achieve a soil: solution ratio of 1:2.5. The water pH was subsequently measured using a combination pH electrode. For moisture content analysis, fresh soil was weighed before and after being dried for one hour. To measure the electrical conductivity of soil water (ECsw1:5), soils were extracted in deionized water for one hour to achieve a soil:water ratio of 1:5. The ECsw1:5 of the extract was subsequently measured using a conductivity meter. The available nitrate-N and ammonia-N, P, and K in rhizosphere soil were determined according to the previous literature [46–47]. Soil micronutrient concentrations were measured using the diethylenetriaminepentaacetic acid (DTPA) extraction method [48]. A total of 10 g of air-dried soil was mixed with 20 mL of DTPA extraction solution (0.005 M DTPA, 0.01 M CaCl2, 0.1 M triethanolamine, pH 7.3) by shaking for 2 hours at room temperature. The liquid supernatants were filtered and subsequently analysed by inductively coupled plasma-optical emission spectrometry (ICP-OES, Optima 7300 DV, PerkinElmer) for Ca, Na, Fe, and Mg concentrations. PCoA analysis with Bray-Curtis distance revealed significant differences in the composition of soil chemical properties between HRS and DRS samples using the Adonis test with an adjusted P value of < 0.05.

Quantification of F. oxysporum abundance

The *Fae* gene (forward primer: 5'-GGCATTTACTCCGCCACTTG-3'; reverse primer: 5'-AGCTCAGCGGCTTCCTATTG-3') was chosen for the determination of *F. oxysporum* abundance in field sampling and pot experiment [49]. Plasmid serial dilutions of ten-fold each containing copies of the 18S rRNA gene from *Saccharomyces cerevisiae* and the internal transcribed spacer (ITS) fragment from *F. oxysporum* were used to generate standard curves (Fig S1). Each PCR reaction, conducted in 8-well tubes, utilized 20 µL of SYBR® Premix Ex TaqTM (TaKaRa, Japan) for amplification of standard and DNA samples in qPCR. Each qPCR reaction included 2 µL of template DNA, 10 µL of SYBR Green Premix Ex Taq (2×), 0.4 µL of each primer, 0.4 µL of ROX Reference Dye II, and sterile water. RT-qPCR followed the manufacturer's protocol: initial denaturation at 95°C for 2 min, followed by 40 cycles of denaturation at 95°C for 10 s, annealing at 60°C for 30 s, and extension at 72°C for 30 s, with a final extension step at 72°C for 10 min. Each sample was subjected to three replicate thermal cycling conditions, and the results were expressed as log copies/g^{-1} of dry soil according to standard procedures.

Total DNA extraction, amplicon, and 16S sequencing

All healthy and diseased *S. miltiorrhiza* plants were collected for analysis. To prepare the samples, the roots were gently shaken to remove loosely attached soil, ensuring that approximately 1 mm of rhizosphere soil remained intact. The roots were then subjected to vortexing in PBS buffer (0.1 M phosphate buffer, 0.15% Tween 80, pH 7.0) for 4 minutes, with the process repeated twice. The resulting suspension was filtered through an 80-mesh sieve to separate root debris, followed by centrifugation at 4000×g for 10 minutes. The small particulate matter obtained after centrifugation was retained as the

rhizosphere soil fraction. Genomic DNA was extracted from each soil sample using the DNeasy® PowerSoil® Kit (QIAGEN GmbH, Germany), following the manufacturer's protocol. DNA concentrations were measured using a Qubit 2.0 fluorometer (Thermo Fisher, USA), and the samples were diluted to achieve consistent concentrations across all rhizosphere DNA samples. For bacterial analysis, the 16S rRNA gene was targeted using primers 515-F (5'-GTGCCAGCMGCCGCGGTAA-3') and 806-R (5'-GGACTACHVGGGTWTCTAAT-3') [50] for all samples. The PCR products obtained were purified and subsequently used to construct sequencing libraries. Sequencing libraries were then prepared and subjected to high-throughput sequencing on the Illumina HiSeq platform at Biozeron (Shanghai, China), generating paired-end reads.

Isolation and identification of rhizosphere Lysobacter

As described by Al-Dhabi and Ishaque *et al.*, *Lysobacter* associated with plants were isolated from the rhizosphere soil of plants grown in the field [51–52]. Healthy *S. miltiorrhiza* plants grown in the field during their growth period were used to isolate *Lysobacter*. The root samples were then suspended in PBS buffer (0.1 M phosphate-buffered saline, 0.15% Tween 80, pH 7.0) and subjected to serial dilution in different culture media for bacterial isolation. The root suspension was diluted in gradients ranging from 10^{-3} to 10^{-7}, and approximately 100 µL of the dilution was plated onto tryptone soy broth (TSB). Individual bacterial colonies were selected based on size, color, and morphology, and then purified by streaking onto tryptone soy agar (TSA) plates. After inoculating the purified single colonies into a 96-well plate, bacterial genomic DNA was extracted using a modified CTAB method following incubation at 95°C for 10 minutes in lysis buffer (0.25% sodium dodecyl sulfate, 0.05 N NaOH). PCR amplification of the bacterial 16S rRNA gene was performed using primers 1492R/274F, with the following cycling conditions: initial denaturation at 95°C for 10 minutes, followed by 30 cycles of denaturation at 95°C for 30 seconds, annealing at 56°C for 30 seconds, extension at 72°C for 90 seconds, and a final extension at 72°C for 10 minutes. Sanger sequencing was conducted by Sangon Biotech (Shanghai, China) using the same primers employed in PCR. All bacterial isolates were identified through BLAST searches against the NCBI database and ITS sequence comparisons [53]. Subsequently, all unique bacterial strains were stored in a 30% glycerol solution and placed in a − 80°C ultra-low temperature freezer (Thermo Scientific, Waltham, MA, USA). Finally, phylogenetic trees were reconstructed using the maximum likelihood method in MEGA version 7.0 [54].

Test of antagonistic effects against F. oxysporum by Lysobacter isolates

Highly pathogenic *F. oxysporum* strain was isolated from root rot *S. miltiorrhiza* rhizosphere soil samples, and then 4 strains of *Lysobacter* isolated from healthy soil samples were evaluated for their antagonistic activity against *F. oxysporum*. The antagonism assay determined the radius of inhibition zone formed between *Lysobacter* strain and *F. oxysporum*. The antagonism assay was performed on an iron-deficient Modified King's B agar medium (MKA, with the same composition as the liquid MKB described previously, supplemented with 15 g L^{-1} agar). A mycelial plug (5 mm in diameter) taken from the actively growing edge of a 5-day-old *F. oxysporum* colony was placed at the center of an MKA plate. Then, 2 µL of

freshly grown bacterial suspension (OD600 ≈ 1.0) of each of the four test *Lysobacter* strains was spot-inoculated onto the agar surface at four equidistant points surrounding the central fungal plug. The smaller the radius of *F. oxysporum*, the stronger the test *Lysobacter* strain resistance to *F. oxysporum*. The antagonism assay against *F. oxysporum* included a total of 4 strains of *Lysobacter*, with three antagonism assays conducted independently for each strain, ultimately selecting candidate strains *Lysobacter* Ly-1 from different species.

Pot experiment to test the ability of Lysobacter Ly-1 to reduce root rot diseases

Pot experiments were established to evaluate the biocontrol potential of *Lysobacter* against root rot caused by *F. oxysporum*. *S. miltiorrhiza* seedlings were cultivated in greenhouse pots (15×15×10 cm) under controlled environmental conditions (30°C, 50% relative humidity). A planting pot was filled with 500 g of substrate. Each treatment consists of 3 replicates, with each replicate containing 6 individually planted seedlings. Subsequently, *Lysobacter* strains Ly-1 were cultured using shake-flask fermentation in TSB medium for a total of 4 days at 30°C. *Lysobacter* fermentation broth was centrifuged at 4000×g for 8 minutes, and the pellets were resuspended in PBS. The suspension was then diluted to approximately 1 × 10^7 cells/mL using a hemocytometer. Two different treatments were designed for the experiment, including Ly-1 (10 mL mixed bacterial solution), and sterile water as a control. Different treatments were applied to 45-day-old seedlings by combined foliar spray and root irrigation. After 15 days, 10 mL of *F. oxysporum* spore suspensions (10^9 CFU/mL) were separately poured into the soil of *S. miltiorrhiza*. At 60 days post *F. oxysporum* inoculation, the root rot disease index was recorded, scored on a 0–4 scale (0: no wilting; 1: 1–25% root area rot; 2: 26–50% root area rot; 3: 51–75% root area rot; and 4: 76–100% root area rot) according to Li et al [55]. The Disease Index (DI) was calculated following the formula:

$$DI = \frac{\sum (Nd \times Cd)}{Ts \times Ad} \times 100\%$$

(Nd: Number of diseased plants at the given disease level, Cd: Corresponding disease level, Ts: Total number of plants surveyed, Ad: Actual highest disease level).

Field experiment

Field experiments were conducted in Yangqiao Town (33°04'N, 115°25'E), Fuyang City, Anhui Province, China, between 2024 and 2025. *S. miltiorrhiza seedlings*, inoculated with Ly-1, were planted in 20 × 100 m plots, with non-inoculated *S. miltiorrhiza* serving as the control. During the seedling stage, *S. miltiorrhiza* plants were sprayed with either Ly-1 (100 L a.i./ha) or water as a control treatment. Each plot contained an average of 15000 *S. miltiorrhiza* plants. All experiments were arranged using a randomized block design, with three replications for both treatment and control groups. At maturity, the aboveground and underground yield were recorded.

Bacterial whole genome sequencing and assembly

Whole-genome sequencing of *Lysobacter* strain Ly-1 was performed using the PromethION platform from Oxford Nanopore Technologies (ONT) at Beijing Tsingke Biotech Co., Ltd. Sequences with a quality score below 10 were removed, yielding a final dataset of 1.09 Gb consisting of 6,666,776 high-quality reads. De novo hybrid assembly of these long reads was carried out using Canu (version 1.6) [56]. Genome annotation of strain Ly-1 was performed using Prokka 1.14.6, a prokaryotic gene prediction tool [57]. Secondary metabolite analysis and prediction for the Ly-1 genome were conducted using the non-redundant protein database (NR) (https://www.ncbi.nlm.nih.gov/refseq/about/non redundant proteins/) [58]. Functional annotation of the genome was performed by mapping to the Kyoto Encyclopedia of Genes and Genomes (KEGG) database, with blastP searches conducted under an E-value threshold of <1e-5 [59]. Finally, a circular genome map was constructed using shinyCircos-V2.0 [60].

Determining the siderophore production and siderophore-mediated effects of Ly-1

We used a modified King's B medium (MKB: 2.5 g L^{-1} K_2HPO_4, 2.5 g L^{-1} $MgSO_4 \cdot 7H_2O$, 15 mL L^{-1} glycerin, and 5.0 g L^{-1} casamino acids, pH 7.2, iron concentration ~ 6 μM) as the iron-limited environment to induce the production of siderophores [61]. To explore the siderophore-mediated effect of *Lysobacter* strain Ly-1 on *F. oxysporum* growth, two treatments were set up to distinguish siderophore-mediated effects: (i) Iron-limited supernatant: 200 μL of cell-free supernatant of Ly-1 collected under iron-limited conditions was added to 2 mL of MKB medium (2.5 g L^{-1} K_2HPO_4, 2.5 g L^{-1} $MgSO_4 \cdot 7H_2O$, 15 mL L^{-1} glycerin, and 5.0 g L^{-1} casamino acids, pH 7.2, iron concentration ~ 6 μM). The initial cultivation of Ly-1 for exudate collection was performed in the same MKB medium (iron-limited or supplemented with 100 μM $FeCl_3$ for iron-rich condition). This supernatant contained total metabolites produced by consortia or consortium members in iron-limited environments, including siderophores. (ii) Iron-rich supernatant: 200 μL of cell-free supernatant collected under the iron-rich (100 μM $FeCl_3$) condition was added to 2 mL of MKB medium. This supernatant contained total metabolites under iron-rich conditions, excluding siderophores produced. Siderophore production in Ly-1 bacterial strains under iron-limited and iron-rich was measured by chrome azurol S (CAS) assays, which gauge the intensity of siderophores chelating ferric ions based on the resulting color change in the reaction mixture [62]. Fungal plugs (5 mm in diameter) were taken from the actively growing edge of a 5-day-old *F. oxysporum* colony on a mother PDA plate. Fungal plugs were added to the two types of medium mentioned above. After five days of shaking incubation, the mycelial mats were harvested by filtration through pre-weighed filter papers, washed thoroughly with distilled water, and dried at 65°C to constant weight. The dry biomass was quantified as the weight difference. The average values of six replicates for both control and treatment were recorded.

Transcriptomic analysis of L. enzymogenes Ly-1 cells

To investigate the molecular response of *L. enzymogenes* Ly-1 to iron availability, transcriptomic profiling was performed on bacterial cells cultured under iron-limited and iron-riched (100 μM $FeCl_3$) conditions,

with three biological replicates for each experimental condition. Total RNA was isolated from the cell cultures using TRIzol® reagent (Invitrogen), following the manufacturer's protocol, and genomic DNA was removed by treatment with DNase (TaKara). Paired-end sequencing libraries were generated and subsequently sequenced on the Illumina NovaSeq 6000 platform (150 bp × 2, Beijing Qingke Biotechnology Co., Ltd.). Raw sequencing reads were processed for quality control and trimming using Trimmomatic (v0.36), applying the parameters SLIDINGWINDOW: 4:15 and MINLEN: 75. Cleaned reads were then mapped to the reference genome in a directional manner using the Rockhopper software [63–65]. Differential gene expression analysis was carried out with the DESeq2 R package (v1.22.1) [66], and the p-values were adjusted using the Benjamini-Hochberg procedure to control the false discovery rate (FDR). Genes exhibiting a Log_2 fold change (Log_2FC) greater than 1 and an FDR of less than 0.05 were considered significantly differentially expressed. KEGG pathway enrichment analysis of the differentially expressed genes was performed using the KEGG Orthology-Based Annotation System (KOBAS 3.0) (http://kobas.cbi.pku.edu.cn/kobas3) to identify the functional pathways associated with these genes.

In vitro experiment to test the effects of $FeCl_3$ on F. oxysporum growth

Two different treatments were designed for the experiment, including iron-limited (MKB medium), and iron-replenish. (i) Iron-limited: Fungal plugs with a diameter of 5 mm were obtained from *F. oxysporum* niveum plates were inoculated into 6-well plates containing 2 mL of MKB medium. (ii) Iron-replenish: Fungal plugs was added to 2 mL of iron-rich MKB medium. This supernatant was supplemented with 25, 100 or 250 μM $FeCl_3$. After five days of shaking incubation, the growth of *F. oxysporum* was determined by dry biomass. The average values of six replicates for both control and treatment were recorded.

Statistical analyses

Statistical analyses were conducted in the R environment (V3.6.0, http://www.r-project.org/). The 'LorMe (V0.4.0)' package in R was used to filter the data to obtain the core microbiome and to analyze alpha diversity indices (including Shannon index and ASVs number index) and conduct network analysis. The 'microeco' package was used to calculate beta diversity differences among different groups, and the Adonis function in R was used to assess the influence of bacterial community structure. Significant differences in the abundance of fungal and bacterial taxa were checked using Log_2FC (fold change) and visualized using 'ggplot2' in R. Wilcoxon test was used to examine the significant differences in the relative abundance of bacterial genus between H and D groups, disease index and biomass, yield, relative abundance of genus and genes, siderophore production, and *F. oxysporum* quantities of different samples. Differences were considered statistically significant at $P < 0.05$, 0.01, and 0.001. one-way analysis of variance (ANOVA) was used to analyze pairwise comparisons of biomass of *F. oxysporum* in different samples.

Data availability

Raw 16S rRNA gene amplicon sequence data derived from all H and D samples in fields are publicly available under NCBI BioProject number PRJNA1222137. The whole-genome sequencing data (Illumina

paired-end and PacBio HiFi) of *Lysobacter enzymogenes* strain Ly-1 have been deposited in the NCBI SRA under BioProject accession number PRJNA1498742, with SRA accession numbers SRR39767230 (Illumina) and SRR39767229 (PacBio), corresponding to BioSample SAMN61855999. The transcriptomic data for *Lysobacter enzymogenes* strain Ly1 are publicly available in the Genome Sequence Archive (GSA) under accession CRA047146 at the National Genomics Data Center (NGDC).

Declarations

Author Contribution

C.Y. and Y.G. contributed equally to this work. C.Y., Y.G., P.R., and W.Q.Z. performed the experiments, analyzed the data, and wrote the main manuscript text. K.G., Q.Z., X.C.W., and W.X.Z. participated in sample collection and field experiments. R.K., Y.X., Q.S., Z.W., and X.F.W. provided conceptual guidance, resources, and critical revision of the manuscript. Y.G. supervised the study. All authors reviewed and approved the final version for publication.

Acknowledgements

This research work was supported by the Fundamental and Interdisciplinary Disciplines Breakthrough Plan of the Ministry of Education of China (JYB2025XDXM703), National Natural Science Foundation of China (Grant No. 42277113, 42377118), the Natural Science Foundation of Jiangsu Province (BK20240194). We are grateful to Dr. Shaohua Gu, Peng Ren and Weiqi Zhang for his kind help in revising and improving the manuscript.

References

1. Panth M, Hassler SC, Baysal-Gurel F, et al. Methods for management of soilborne diseases in crop production. Agriculture, 2020; 10: 16.
2. Li C, Shang H, Su X, et al. Isolation and identification of root rot pathogens of *Salvia miltiorrhiza* and fungicide screening. Shandong Agric. Sci, 2022, 54: 119–125.
3. Wang B Q. Salvia miltiorrhiza: Chemical and pharmacological review of a medicinal plant. J Med Plants Res, 2010, 4(25): 2813–2820.
4. Yang J, Wen Y, GAO S, et al. Identification of pathogens causing *Salvia miltiorrhiza* root rot disease in henan province. Journal of Henan Agricultural Sciences, 2021, 50(10): 92.
5. Sa R, He S, Han D, et al. Isolation and identification of a new biocontrol bacteria against *Salvia miltiorrhiza* root rot and optimization of culture conditions for antifungal substance production using response surface methodology. BMC microbiology, 2022, 22(1): 231.
6. Williamson-Benavides B A, Dhingra A. Understanding root rot disease in agricultural crops. Horticulturae, 2021, 7(2): 33.

7. Lambers H, Mougel C, Jaillard B, et al. Plant-microbe-soil interactions in the rhizosphere: an evolutionary perspective. 2009.
8. Berg G, Smalla K. Plant species and soil type cooperatively shape the structure and function of microbial communities in the rhizosphere. FEMS microbiology ecology, 2009, 68(1): 1–13.
9. Shen Z, Thomashow LS, Ou Y, et al. Shared core microbiome and functionality of key taxa suppressive to banana Fusarium wilt. Research, 2022.
10. Kumar S, Gupta O M. Expanding dimensions of plant pathology. JNKVV Res. J, 2012, 46(3): 286–293.
11. Li B, Yang P, Feng Y, et al. Rhizospheric microbiota of suppressive soil protect plants against *Fusarium solani* infection. Pest Management Science, 2024.
12. Gu S, Wei Z, Shao Z, et al. Competition for iron drives phytopathogen control by natural rhizosphere microbiomes. Nature Microbiology, 2020, 5(8): 1002–1010.
13. Compant S, Samad A, Faist H, et al. A review on the plant microbiome: ecology, functions, and emerging trends in microbial application. Journal of advanced research, 2019, 19: 29–37.
14. Coats V C, Rumpho M E. The rhizosphere microbiota of plant invaders: an overview of recent advances in the microbiomics of invasive plants. Frontiers in microbiology, 2014, 5: 368.
15. Song J, Xi X, Qian X, et al. Revealing the microbial composition changes and relationship with Fusarium caused by rot disease in the Crocus sativus L. Annals of Microbiology, 2024, 74(1): 24.
16. Gu S, Wei Z, Shao Z, et al. Competition for iron drives phytopathogen control by natural rhizosphere microbiomes. Nature Microbiology, 2020, 5(8): 1002–1010.
17. Compant S, Samad A, Faist H, et al. A review on the plant microbiome: ecology, functions, and emerging trends in microbial application. Journal of advanced research, 2019, 19: 29–37.
18. Brescia F, Pertot I, Puopolo G. *Lysobacter*[M]//Beneficial microbes in agro-ecology. Academic Press, 2020: 313–338.
19. Gómez Expósito R, Postma J, Raaijmakers J M, et al. Diversity and activity of *Lysobacter* species from disease suppressive soils. Frontiers in microbiology, 2015, 6: 1243.
20. O'SULLIVAN J, McCULLOUGH J E, Tymiak A A, et al. Lysobactin, a novel antibacterial agent produced by *Lysobacter* sp. I. Taxonomy, isolation and partial characterization. The journal of antibiotics, 1988, 41(12): 1740–1744.
21. Bernhard F, Demel G, Soltani K, et al. Identification of genes encoding for peptide synthetases in the gram-negative bacterium *Lysobacter* sp. ATCC 53042 and the fungus Cylindrotrichum oligospermum. DNA Sequence, 1996, 6(6): 319–330.
22. Lou L, Qian G, Xie Y, et al. Biosynthesis of HSAF, a tetramic acid-containing macrolactam from *Lysobacter enzymogenes*. Journal of the American Chemical Society, 2011, 133(4): 643–645.
23. QIAN G, HU B, JIANG Y, et al. Identification and characterization of *Lysobacter enzymogenes* as a biological control agent against some fungal pathogens. Agricultural Sciences in China, 2009, 8(1): 68–75.

24. Nian J, Yu M, Bradley C A, et al. *Lysobacter enzymogenes* strain C3 suppresses mycelium growth and spore germination of eight soybean fungal and oomycete pathogens and decreases disease incidences. Biological Control, 2021, 152: 104424.
25. Lin L, Yang Z, Tao M, et al. *Lysobacter enzymogenes* prevents Phytophthora infection by inhibiting pathogen growth and eliciting plant immune responses. Frontiers in plant science, 2023, 14: 1116147.
26. Liu Y, Qiao J, Liu Y, et al. Characterization of *Lysobacter capsici* strain NF87–2 and its biocontrol activities against phytopathogens. European Journal of Plant Pathology, 2019, 155: 859–869.
27. Mendes R, Garbeva P, Raaijmakers J M. The rhizosphere microbiome: significance of plant beneficial, plant pathogenic, and human pathogenic microorganisms. FEMS microbiology reviews, 2013, 37(5): 634–663.
28. Colombo C, Palumbo G, He J Z, et al. Review on iron availability in soil: interaction of Fe minerals, plants, and microbes. Journal of soils and sediments, 2014, 14: 538–548.
29. Lemanceau P, Expert D, Gaymard F, et al. Role of iron in plant–microbe interactions. Advances in botanical research, 2009, 51: 491–549.
30. Kurth C, Kage H, Nett M. Siderophores as molecular tools in medical and environmental applications. Organic & biomolecular chemistry, 2016, 14(35): 8212–8227.
31. Carroll C S, Moore M M. Ironing out siderophore biosynthesis: a review of non-ribosomal peptide synthetase (NRPS)-independent siderophore synthetases. Critical reviews in biochemistry and molecular biology, 2018, 53(4): 356–381.
32. Yu S, Teng C, Liang J, et al. Characterization of siderophore produced by *Pseudomonas syringae* BAF. 1 and its inhibitory effects on spore germination and mycelium morphology of *Fusarium oxysporum*. Journal of Microbiology, 2017, 55: 877–884.
33. Philpott C C. Iron uptake in fungi: a system for every source. Biochimica et Biophysica Acta (bba)-molecular cell research, 2006, 1763(7), 636–645.
34. Liu Y, Kong D, Wu H L, et al. Iron in plant–pathogen interactions. Journal of Experimental Botany, 2021, 72(6), 2114–2124.
35. Caza M, Kronstad J W. Shared and distinct mechanisms of iron acquisition by bacterial and fungal pathogens of humans. Frontiers in cellular and infection microbiology, 2013, 3, 80.
36. Leal Jr S M, Roy S, Vareechon C, et al. Targeting iron acquisition blocks infection with the fungal pathogens *Aspergillus fumigatus* and *Fusarium oxysporum*. PLoS pathogens, 2013, 9(7): e1003436.
37. Hungate B A, Marks J C, Power M E, et al. The functional significance of bacterial predators. Mbio, 2021, 12(2): 10.1128/mbio. 00466 – 21.
38. Seccareccia I, Kost C, Nett M. Quantitative analysis of *Lysobacter* predation. Applied and Environmental Microbiology, 2015, 81(20): 7098–7105.
39. Konhauser K O, Kappler A, Roden E E. Iron in microbial metabolisms. Elements, 2011, 7(2): 89–93.

40. Heidari Z, Faezi Ghasemi M, Modiri L. The synergistic antibacterial effect of bacteriocin produced by *Lactobacillus casei* ATCC 39392 and iron oxide nanoparticles (IONPs) on selected foodborne pathogens. International Journal of Molecular and Clinical Microbiology, 2020, 10(1), 1301–1311.
41. Garénaux A, Caza M, Dozois C M. The Ins and Outs of siderophore mediated iron uptake by extra-intestinal pathogenic *Escherichia coli*. Veterinary microbiology, 2011, 153(1–2), 89–98.
42. Miller A L, Li S, Eichhorn C D, et al. Identification and biosynthetic study of the siderophore lysochelin in the biocontrol agent *Lysobacter enzymogenes*. Journal of Agricultural and Food Chemistry, 2023, 71(19): 7418–7426.
43. Tang B, Wang B, Xu Z, et al. Iron ions regulate antifungal HSAF biosynthesis in *Lysobacter enzymogenes* by manipulating the DNA-binding affinity of the ferric uptake regulator (Fur). Microbiology Spectrum, 2023, 11(5): e00617-23.
44. Mozdzan M, Szemraj J, Rysz J, et al. Anti-oxidant activity of spermine and spermidine re-evaluated with oxidizing systems involving iron and copper ions. The international journal of biochemistry & cell biology, 2006, 38(1): 69–81.
45. Hamamoto H, Urai M, Ishii K, et al. Lysocin E is a new antibiotic that targets menaquinone in the bacterial membrane. Nature chemical biology, 2015, 11(2), 127–133
46. Zilio M, Motta S, Tambone F, et al. The distribution of functional N-cycle related genes and ammonia and nitrate nitrogen in soil profiles fertilized with mineral and organic N fertilizer. PLoS One, 2020, 15(6): e0228364.
47. Liu X, Ma Y, Manevski K, et al. Biochar and alternate wetting-drying cycles improving rhizosphere soil nutrients availability and tobacco growth by altering root growth strategy in Ferralsol and Anthrosol. Science of the Total Environment, 2022, 806: 150513.
48. Sidhu G S, Sharma B D. Diethylenetriaminepentaacetic acid-extractable micronutrients status in soil under a rice-wheat system and their relationship with soil properties in different agroclimatic zones of indo-gangetic plains of India. Communications in Soil Science and Plant Analysis, 2010, 41: 29–51.
49. Xing Y, Chen Y, Feng CC, et al. Establishment and application of real-time quantitative PCR detection system for the pathogenic *Fusarium oxysporum* causing *Astragalus membranaceus* var. mongholicus root rot. Journal of Agricultural Biotechnology. 2024, 32: 720–729.
50. Shi G, Hu J, Zhang S, et al. The application of exogenous Se improved the remediation efficiency of *Lolium multiflorum* Lam grown in nonylphenol-Cd Co-contaminated soil. Journal of Environmental Chemical Engineering, 2022, 10(6), 108962.
51. Singh H, Won K H, Du J, et al. Lysobacter agri sp. nov., a bacterium isolated from soil. Antonie van Leeuwenhoek, 2015, 108: 553–561.
52. Park J H, Kim R, Aslam Z, et al. Lysobacter capsici sp. nov., with antimicrobial activity, isolated from the rhizosphere of pepper, and emended description of the genus Lysobacter. International Journal of Systematic and Evolutionary Microbiology, 2008, 58(2): 387–392.

53. Johnson M, Zaretskaya I, Raytselis Y, et al. NCBI BLAST: a better web interface. Nucleic Acids Res. 2008, 36: W5-9.
54. Kumar S, Stecher G, Tamura K. MEGA7: molecular evolutionary genetics analysis version 7.0 for bigger datasets. Mol Biol Evol. 2016, 33: 1870–4.
55. Li GQ, Huang HC, Miao HJ, et al. Biological control of sclerotinia diseases of rapeseed by aerial applications of the mycoparasite *Coniothyrium minitans*. Eur. J. Plant Pathol. 2006, 114: 345–355.
56. Koren S, Walenz BP, Berlin K, Miller JR, Bergman NH, Phillippy AM. Canu: scalable and accurate long-read assembly via adaptive k -mer weighting and repeat separation. Genome Res. 2017, 27: 722–36.
57. Seemann T. Prokka: rapid prokaryotic genome annotation. Bioinformatics. 2014, 30: 2068–9.
58. Kallberg Y, Persson B. KIND-a non-redundant protein database. Bioinformatics (oxford, England), 1999, 15(3): 260–261.
59. Kanehisa M, Goto S. KEGG: kyoto encyclopedia of genes and genomes. Nucleic acids research, 2000, 28(1): 27–30.
60. Wang Y, Jia L, Tian G, et al. shinyCircos-V2.0: Leveraging the creation of Circos plot with enhanced usability and advanced features. iMeta. 2023, 2.
61. Höfte M, Buysens S, Koedam N, et al. Zinc affects siderophore-mediated high affinity iron uptake systems in the rhizosphere Pseudomonas aeruginosa 7NSK2. Biometals, 1993, 6: 85–91.
62. Schwyn B, Neilands J B. Universal chemical assay for the detection and determination of siderophores. Analytical biochemistry, 1987, 160(1): 47–56.
63. Koren S, Walenz BP, Berlin K, Miller JR, Bergman NH, Phillippy AM. Canu: scalable and accurate long-read assembly via adaptive k -mer weighting and repeat separation. Genome Res. 2017, 27: 722–36.
64. Seemann T. Prokka: rapid prokaryotic genome annotation. Bioinformatics. 2014, 30: 2068–9.
65. Brian T. A computational system for identifying operons based on RNA-seq data, Methods, 2020, 176: 62–70.
66. Brian T. De novo assembly of bacterial transcriptomes from RNA-seq data. Genome Biology, 2015, 16: 1.

Figures

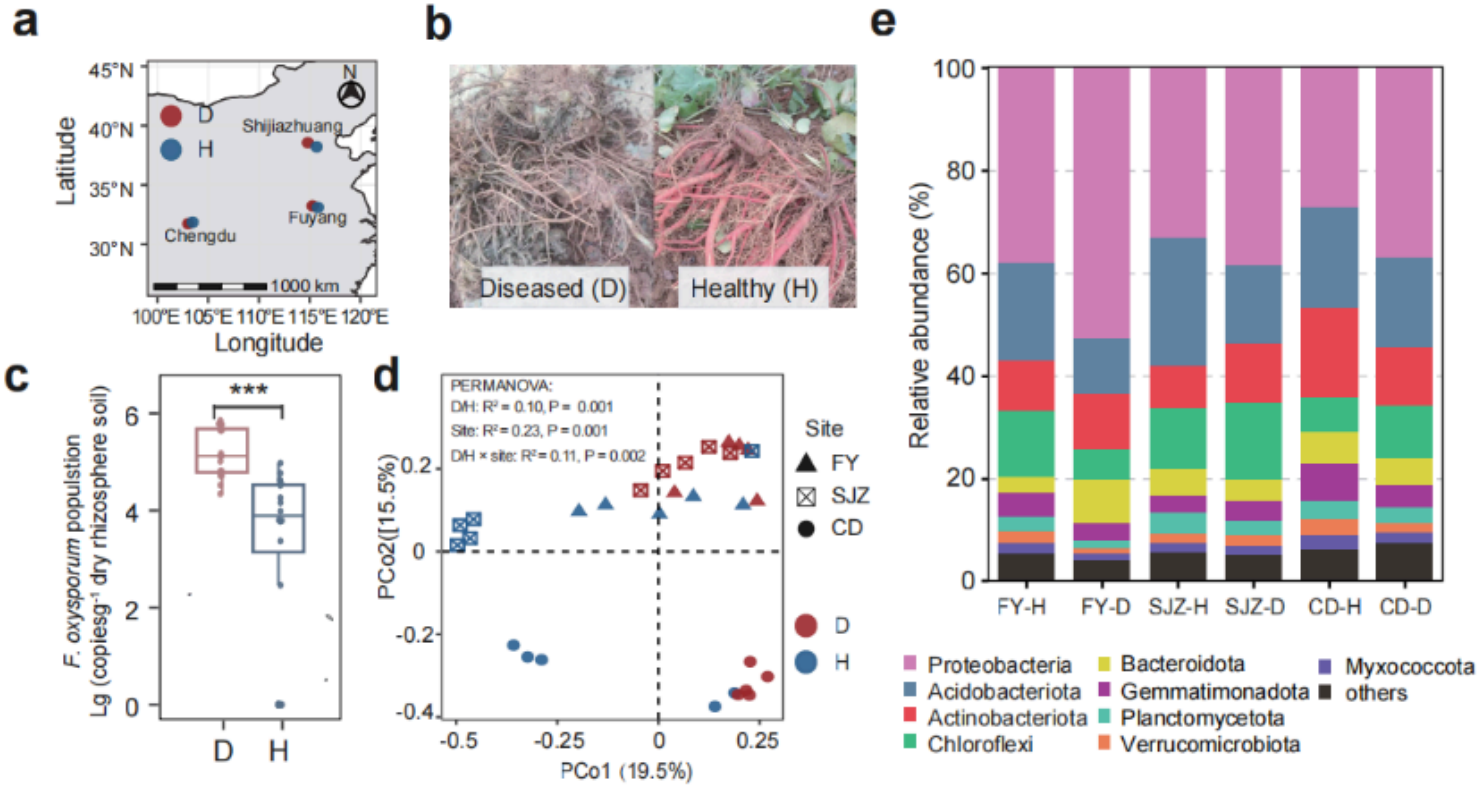


Figure 1

Comparative analysis of rhizosphere microbiomes between root rot-diseased (D) and healthy (H) *Salvia miltiorrhiza* plants. a) Geographical distribution of sampling sites across major *S. miltiorrhiza* production regions in China. b) Representative field phenotypes showing characteristic symptoms of D versus H plants. c) Quantitative comparison of *F. oxysporum* gene copies in rhizosphere soils, with box plots demonstrating significantly higher pathogen abundance in diseased samples (***$P < 0.001$, Wilcoxon rank-sum test). d) Beta-diversity patterns revealed by Principal Coordinates Analysis (PCoA) based on ASVs, showing distinct clustering of microbial communities between D and H groups. e) The relative abundance of the top 10 bacterial phylum.

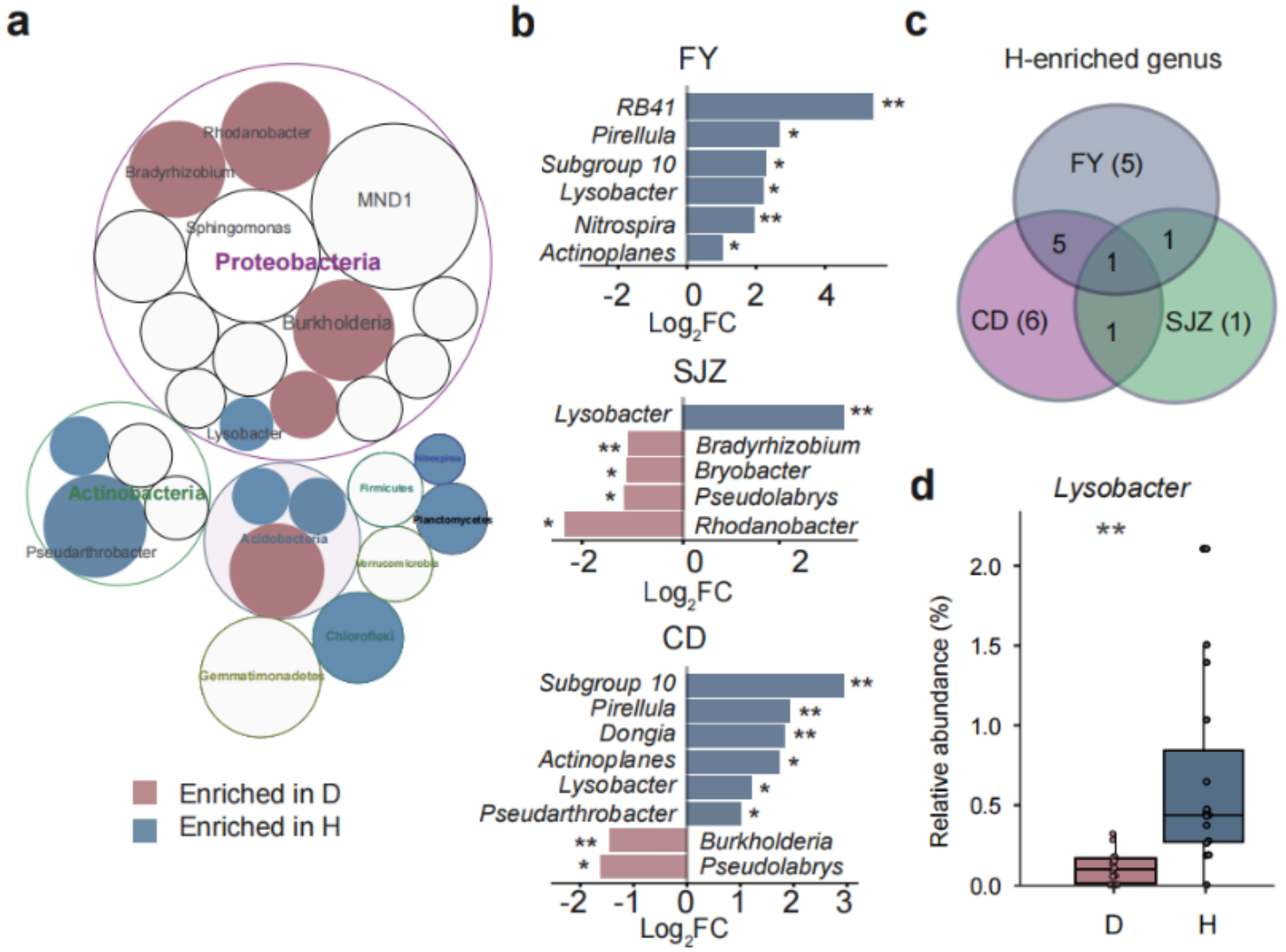


Figure 2

Identification of core microbiome biomarkers associated with rhizosphere health status. a) Taxonomic differences for the core bacterial microbiome between D and H rhizosphere soils are based on 16S rRNA gene sequences. The outside circles to inner circles represent phylum and genus level, respectively. Solid circles represent enriched genera. b) Site-specific enrichment patterns of core bacterial genera, displaying $\log_2$-transformed fold-changes in relative abundance between healthy (H, blue) and diseased (D, red) rhizospheres. Statistical significance was determined by Wilcoxon signed-rank tests with exact P-values annotated. c) Consensus healthy-enriched core genera consistently identified across all sampling locations. d) Differential abundance of the core genus *Lysobacter*, showing significantly higher colonization in healthy rhizospheres (*P < 0.05, **P < 0.01, Wilcoxon rank-sum test).

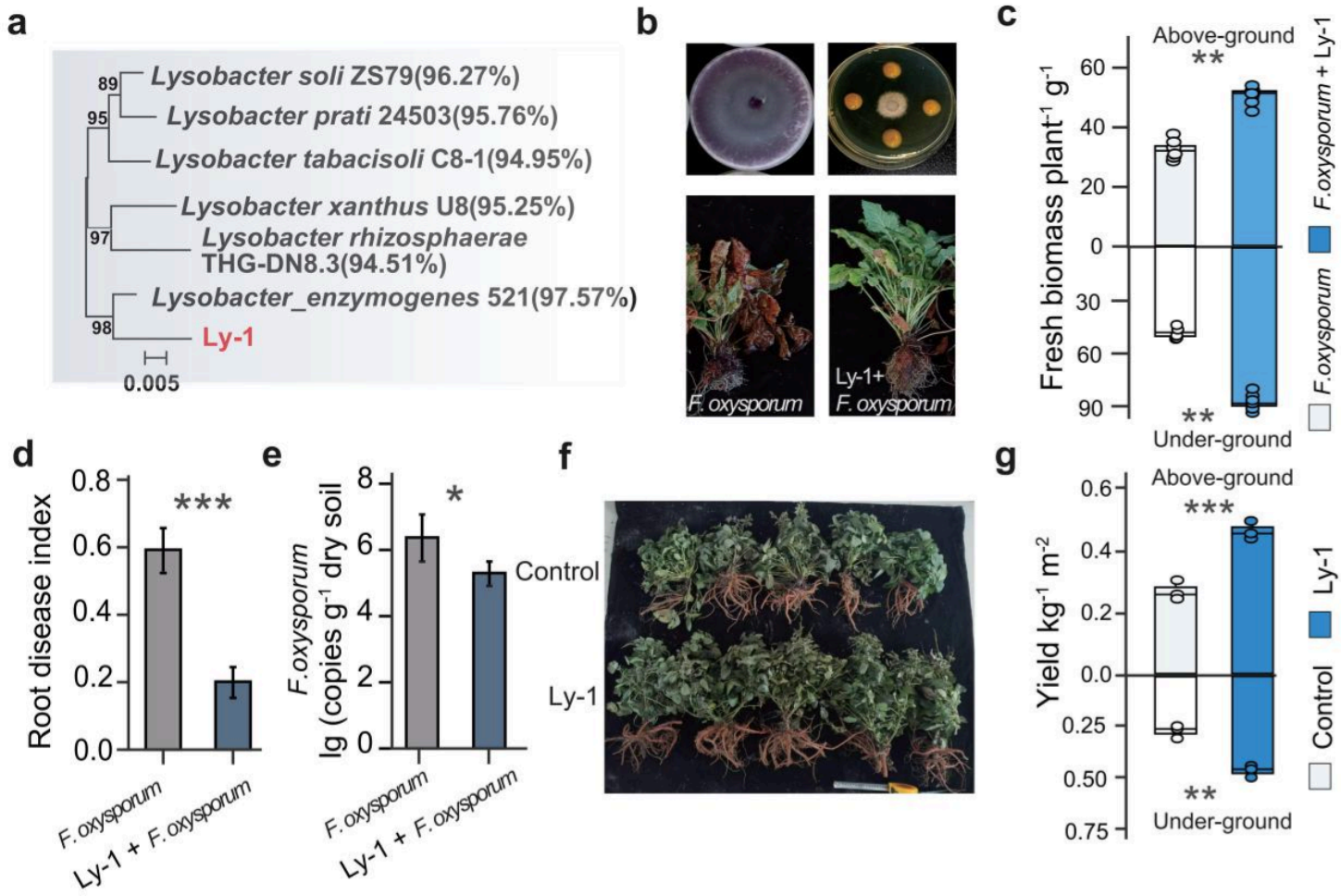


Figure 3

Biocontrol efficacy and growth-promoting effects of *L. enzymogenes* Ly-1 against *F. oxysporum*-induced root rot. a) Phylogenetic characterization of strain Ly-1 through neighbor-joining analysis, with reference sequences from NCBI (species names and accession numbers). Node support values represent bootstrap percentages (1,000 replicates). b) Top: Antagonistic activity demonstrated by co-culture assay on potato dextrose agar (PDA), showing *F. oxysporum* colony morphology (left) versus Ly-1-mediated inhibition zone (right); Bottom: Comparative phenotypes of *S. miltiorrhiza* leaves/roots under pathogen alone (Fo) versus Ly-1 biocontrol (Ly-1+Fo) (pot experiment). c) Histogram showing the above-ground (above the horizontal axis) and under-ground (below the horizontal axis) fresh biomass of *S. miltiorrhiza* plants treated with *Lysobacter* (pot experiment). d) Disease severity index reduction in Ly-1-treated plants (pot experiment). e) *F. oxysporum* gene copy numbers in rhizosphere soils (pot experiment). f) Representative root health status across treatments (field experiment). g) Yield improvement metrics for above-ground (above the horizontal axis) and under-ground (below the horizontal axis) harvests (field experiment). Statistical annotations: *P< 0.05, **P < 0.01, ***P < 0.001 (Wilcoxon rank-sum test, Ly-1 vs control).

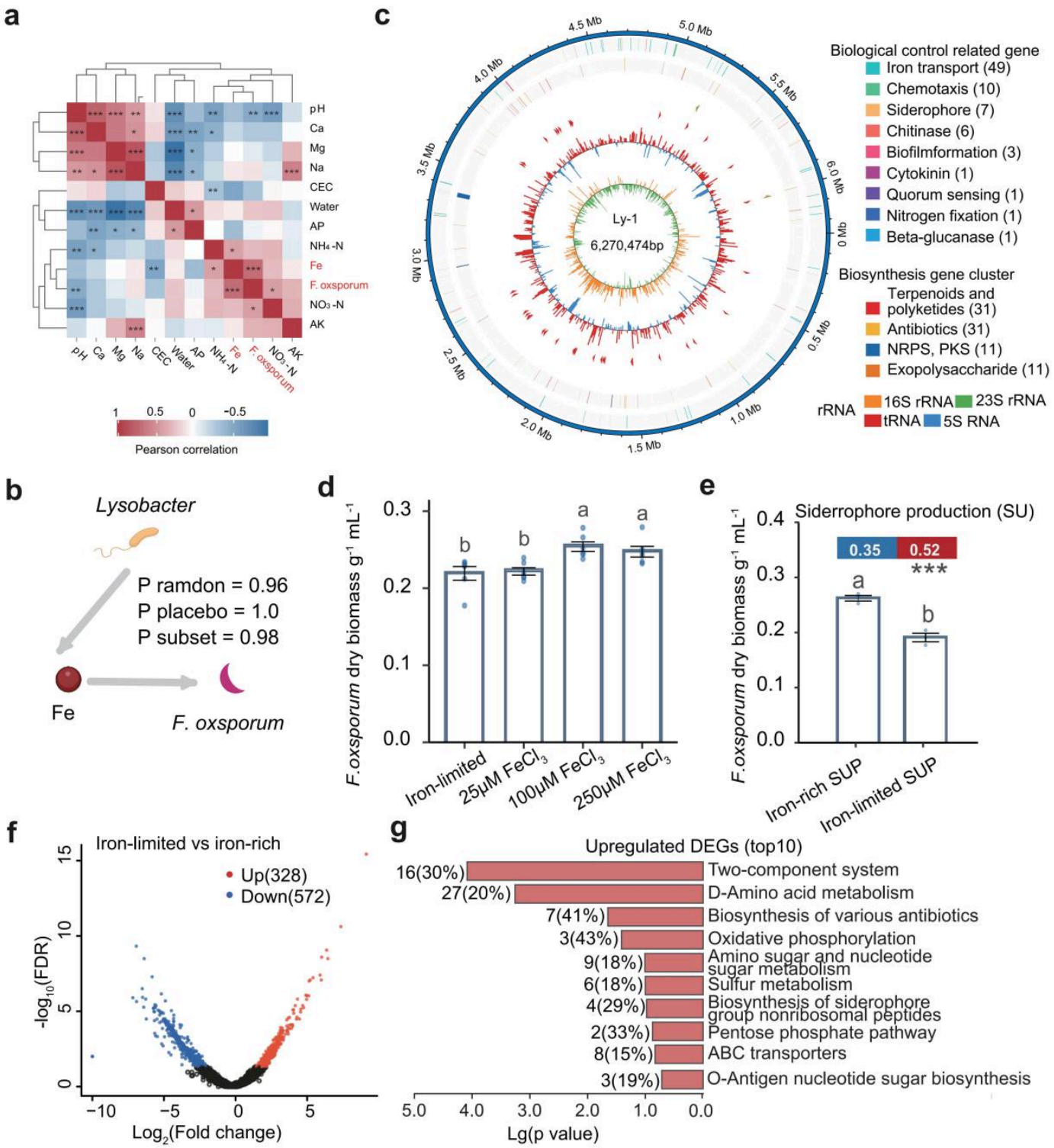


Figure 4

Genome Map and Functional Characteristics of *Lysobacter* Ly-1. a) The heatmap showing the Pearson correlation between different soil physicochemical factors and *F. oxysporum* (*P <0.05, **P <0.01, ***P <0.001), The values are the correlation coefficient R^2 the different factors. b) The results of causal model. “P random”, “P placebo”, “P subset” represent P averange approach and clustered multiple threshold approach, respectively. c) Complete genome of Ly-1 and functional annotations, the circular genome

map (inner to outer) illustrates the genomic architecture, including 16S rRNA, 23S rRNA, tRNA, and 5S rRNA loci, along with protein-coding genes. Functional annotation was performed using two complementary approaches: KEGG-based secondary metabolism prediction: Identified gene clusters associated with antibiotics biosynthesis (31 genes), terpenoid and polyketide biosynthesis (31 genes), exopolysaccharide biosynthesis (11 genes), and nonribosomal peptide synthetase (NRPS)/polyketide synthase (PKS) pathways (11 genes). NR_tophit-based functional annotation: Highlighted genes linked to biocontrol and plant-growth promotion, including iron transport (49 genes), chemotaxis (10 genes), siderophore synthesis (7 genes), chitinase production (6 genes), biofilm formation (3 genes), cytokinin synthesis (1 gene), quorum sensing (1 gene), nitrogen fixation (1 gene), and β-glucanase activity (1 gene). d) Iron-mediated growth rescue: Mycelial biomass under iron-deficient conditions supplemented with different concentrations of $FeCl_3$. Letters denote statistical groups (Tukey's HSD, $p < 0.05$). e) Antifungal activity of Ly-1 supernatant against *F. oxysporum* under three treatments: Iron-rich SUP, cultured in MKB (Modified King's B) medium supplemented with cell-free supernatant from Ly-1 grown under iron-rich conditions (100 μM $FeCl_3$); Iron-limited SUP, cultured in MKB medium supplemented with Ly-1 supernatant from iron-limited conditions. Letters denote statistical groups (Tukey's HSD, $p < 0.05$). f) Volcano plot of differentially expressed genes (DEGs) in Ly-1 cultured in iron-limited conditions (iron-limited) versus iron-rich conditions (iron-rich). Thresholds: $|log2FC| > 1$, $p < 0.05$. g) KEGG enrichment analysis of DEGs showing functional changes induced by iron-limited conditions. Bubble size represents gene counts per pathway, with log10-transformed p-values on the x-axis.

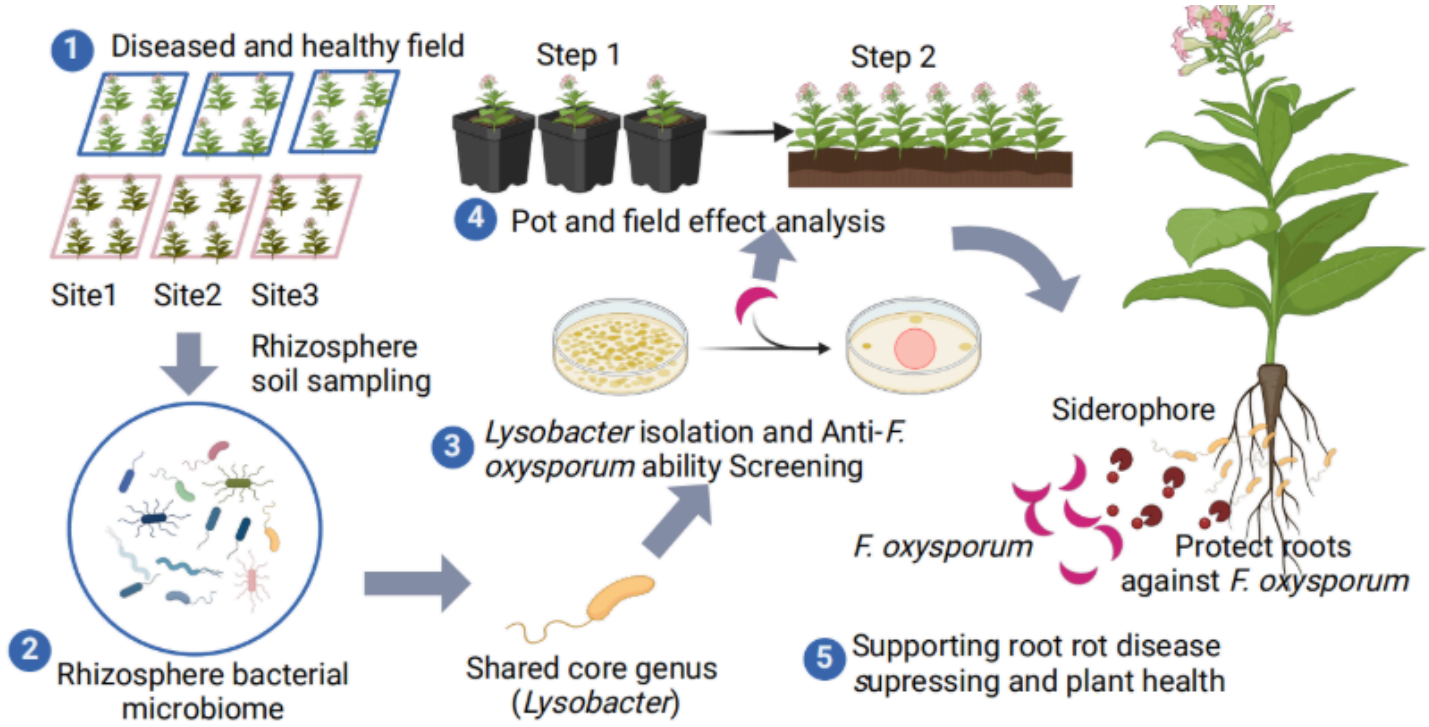


Figure 5

Conceptual model illustrating the shared core strain and potential mechanism in rhizosphere soils of *Salvia miltiorrhiz*a. Picture summarizing the features of core microbiome in separately located disease-

suppressive soils and potential mechanism of disease-suppressive microbes against fungal pathogen growth and subsequent plant infection.

Supplementary Files

This is a list of supplementary files associated with this preprint. Click to download.

- TableS1.xlsx
- TableS2.xlsx
- Supplymentalfigures.docx